Remote Sensing of Environment 274 (2022) 112991

Contents lists available at ScienceDirect

Remote Sensing of Environment

journal homepage: www.elsevier.com/locate/rse

Evaluating recovery metrics derived from optical time series over tropical forest ecosystems

Wanda De Keersmaecker [a,b,*], Pablo Rodríguez-Sánchez [c], Milutin Milenković [a], Martin Herold [a], Johannes Reiche [a], Jan Verbesselt [a]

[a] Laboratory of Geo-Information Science and Remote Sensing, Wageningen University, Wageningen, the Netherlands
[b] Vlaamse Instelling Voor Technologisch Onderzoek (VITO) Research Organisation, 2400 Mol, Belgium
[c] Netherlands eScience Center, Amsterdam, the Netherlands

ARTICLE INFO

Editor: Dr Marie Weiss

Keywords:
Tropical forest
Recovery
Resilience
Landsat
Simulation
Disturbance
Sensitivity

ABSTRACT

An increase in the frequency and severity of disturbances (such as forest fires) is putting pressure on the resilience of the Amazon tropical forest; potentially leading to reduced ability to recover and to maintain a functioning forest ecosystem. Dense and long-term satellite time series approaches provide a largely untapped data source for characterizing disturbance- recovery forest dynamics across large areas and varying types of forests and conditions. Although large-scale forest recovery capacity metrics have been derived from optical satellite image time series and validated over various ecosystems, their sensitivity to disturbance (e.g. disturbance magnitude, disturbance timing, and recovery time) and environmental data characteristics (e.g. noise magnitude, seasonality, and missing values) are largely unknown. This study proposes an open source simulation framework based on the characteristics of sampled original satellite image time series to (i) compare the reliability of recovery metrics, (ii) evaluate their sensitivity with respect to environmental and disturbance characteristics, and (iii) evaluate the effect of pre-processing techniques on the reliability of the recovery metrics for abrupt disturbances, such as fires, in the Amazon basin forests. The effect of three pre-processing techniques were evaluated: changing the temporal resolution, noise removal techniques (such as time series smoothing and segmenting), and using a varying time span after the disturbance to calculate recovery metrics. Here, reliability is quantified by comparing derived and theoretical values of the recovery metrics (RMSE and R^2). From the three recovery metrics evaluated, the Year on Year Average (YrYr) and the Ratio of Eighty Percent (R80p) are more reliable than the Relative Recovery Index (RRI). Time series segmentation tends to improve the reliability of recovery metrics. Recovery metrics derived from temporal dense Landsat time series tend to show a higher reliability than those derived from time series aggregated to quarterly or annual values. Although the framework is demonstrated on Landsat time series of the Amazon tropical forest, it can be used to perform such test on other datasets and ecosystems.

1. Introduction

Disturbances are inherently linked to the functioning of tropical ecosystems and are necessary to sustain their species composition, biodiversity and structure (Durigan and Ratter, 2016; Kelly and Brotons, 2017; Schmidt et al., 2018). Yet, due to anthropogenic and climatic pressures, there is an increase in the frequency and severity of disturbances, such as large-scale wildfires, in tropical areas (Alencar et al., 2015; Fidelis et al., 2018). Wildfires are posing problems in diverse ecosystems, going from tropical Savannah, to more moist, tropical forest (Silva Junior et al., 2019). Deforestation and fragmentation opens-up tropical forest, resulting in drier conditions with higher fuel load (Taubert et al., 2018; Hansen et al., 2020). This, combined with a higher drought frequency, makes the forest more susceptible to intense wildfires (Silva Junior et al., 2018; Brando et al., 2020).

The increase in large-scale fire occurrence has severe socio-economic and ecological impacts and serves as a positive feedback mechanism on climate change by increasing carbon emissions (Aragao et al., 2018; Aragao and Shimabukuro, 2010). For example, during droughts like those in 2015, the gross emissions from forest fires in the Amazon are

* Corresponding author at: Laboratory of Geo-Information Science and Remote Sensing, Wageningen University, Wageningen, the Netherlands.
E-mail address: wanda.dekeersmaecker@vito.be (W. De Keersmaecker).

https://doi.org/10.1016/j.rse.2022.112991
Received 17 December 2020; Received in revised form 24 November 2021; Accepted 6 March 2022
Available online 14 March 2022

more than half as large as those from old-growth forest deforestation (Aragao et al., 2018). Moreover, the interaction between altered fire regimes and other direct and indirect anthropogenic impacts can affect the resilience of tropical forests and Savannah systems, i.e. their ability to remain in their current state (Flores et al., 2017; Hirota et al., 2011; Staal et al., 2018; Wuyts et al., 2017). There is as such an urgent need to monitor the recovery capacity of tropical forests and systems from these disturbances. This need is strengthened by the fact that slow recovery from local disturbances is potentially an indicator for the loss of large-scale resilience (van de Leemput et al., 2018).

Assessing recovery capacity in tropical areas is however challenging from a practical point of view given the low accessibility of many tropical areas combined with the need for a long-term, dense record of consistent measurements over large areas; that satellite data can increasingly provide (Pettorelli et al., 2014). Many studies have already explored the potential of remote sensing time series to map the recovery capacity of vegetated systems at large spatial scales (Frazier et al., 2015, 2018; Hislop et al., 2018; Nguyen et al., 2018; Verbesselt et al., 2016; White et al., 2017, 2018). Many of these studies focus on recovery metrics after a particular disturbance (e.g. wildfire) by comparing the post-fire vegetation state with the state prior to and during the disturbance (Frazier et al., 2018; White et al., 2017). For example, the Ratio of Eighty Percent (R80p), a recovery metric that compares the post-disturbance and pre-disturbance state, gives insight into the level of recovery to the original state (Pickell et al., 2016; Frazier et al., 2018). The Relative Recovery Index (RRI) relates the recovery magnitude to the disturbance magnitude and the Year on Year Average metric is related to the post-disturbance slope (Kennedy et al., 2012; Frazier et al., 2018). The metrics are often derived from time series of optical satellite images over forest areas. More specifically, the normalized burn ratio (NBR) index, given by the normalized difference between the near infrared and shortwave infrared bands of a multi-spectral satellite image (Key, 2006), is frequently used. NBR dynamics over forests relate to changes in structure and moisture content, and have proven to be more sensitive to forest recovery dynamics as compared to other vegetation indices (Hislop et al., 2018). The index is frequently derived from Landsat time series, often in combination with techniques to enhance the signal to noise ratio, such as the use of an annual best available pixel approach, segmentation of the time series, or function fitting (Frazier et al., 2015; Kennedy et al., 2010; Nguyen et al., 2018).

Landsat data enable the study of time series with a long time span (from the 1970's till now) at a relatively high spatial resolution (30 m), but have a rather low revisit frequency (16 days) (Wulder et al., 2012). With the launch of two Sentinel-2 satellites in 2015 and 2017, an increased combined revisit time of 5 days with an enhanced spatial resolution up to 10 m can be reached (Drusch et al., 2012). Moreover, Sentinel-1 Synthetic Aperture Radar (SAR) A and B satellites since 2014 and 2016, respectively, provide high resolution C-band SAR time series (~10 m) with a frequent revisit time (6–12 days) that are related to vegetation structure and moisture content (Vreugdenhil et al., 2018; Torres et al., 2012). The Sentinel time series are however still relatively short, and the restricted time span available to quantify the pre- and post-disturbance state is potentially limiting their usage for forest recovery studies. Hence, initiatives to combine Sentinel-2 with Landsat data to generate Harmonized Landsat-Sentinel time series are promising to study long-term vegetation disturbance and recovery dynamics (Claverie et al., 2018).

Although forest recovery metrics derived from optical data have been validated over various ecosystems using in situ measurements (e.g. White et al., 2019), visual assessment of the time series (Kennedy et al., 2012), and linked them to airborne laser scanner data (White et al., 2018; Senf et al., 2019) and high resolution imagery (Storey et al., 2016; Viana-Soto et al., 2020), the reliability of recovery metrics and their sensitivity to data characteristics (e.g. noise level, seasonal amplitude, disturbance magnitude and timing) are not known. For example, it is unclear for which magnitude of disturbance impact the disturbance-recovery signal is strong enough to dominate the noise level and the recovery capacity can accurately be measured. Gaining insight in the reliability and sensitivity of recovery metrics is thus critically needed for recovery analyses. Yet, in situ data that support an in-depth sensitivity analysis over a wide range of forest disturbance-recovery dynamics are not available in the tropics.

There is a large variety of forest conditions, disturbance types and factors influencing the pattern of forest recovery over large forest areas such as those in the Amazon basin. To better understand the abilities and approaches for using satellite time series to characterize those, one would ideally use a series of local case studies with long-term in situ measurements. However, in absence of such in situ reference data - which is the case for the Amazon - a simulation framework is the way forward to get insight in the sensitivity and reliability of newly developed or existing methods (e.g. De Keersmaecker et al., 2014; Awty-Carroll et al., 2019; Abel et al., 2019). Since the characteristics of the simulated time series can be controlled, the validation of methods is facilitated and the sensitivity of the method can be evaluated with respect to a particular, isolated time series characteristic (Lhermitte et al., 2011; Verbesselt et al., 2010). Reliability can for instance be quantified by comparing the derived and theoretical values of the recovery metrics (using RMSE or R^2). Moreover, a wide gradient of disturbance - recovery dynamics and environmental time series characteristics can easily be covered.

Using a simulation framework, this study aims to evaluate the reliability and sensitivity of tropical forest recovery metrics derived from Landsat time series after an abrupt disturbance, such as fire. Our objectives are to:

- Compare the reliability of different recovery metrics under the same conditions.
- Evaluate the effect of individual environmental and disturbance characteristics on the reliability of recovery metrics. Here, environmental characteristics denote the noise level, seasonal amplitude, and fraction of missing values. The disturbance characteristics include the disturbance magnitude, disturbance timing, and recovery period.
- Assess which pre-processing steps are most effective to increase the reliability of the recovery metrics. In this study, we evaluate the effect of temporal aggregation methods and noise reduction techniques (i.e. time series smoothing and segmenting). Given that time series of recently launched sensors like the Sentinels only cover a short time span, we additionally aimed to compare the reliability of recovery metrics when the data covers a short versus long time span and hence a short versus long post-recovery period is available.

Our approach is applied using data from the Amazon forest area but the general framework is applicable for other regions and data settings.

2. Methods

In order to evaluate the reliability and sensitivity of the recovery metrics, we developed a simulation framework that relies on time series characteristics from sampled undisturbed tropical forest pixels (Fig. 1). By using these characteristics to simulate time series, we ensured that the properties of the simulated time series are situated within a realistic range. The framework allows to simulate time series of disturbed forests, where the following environmental and disturbance parameters can be controlled: amplitude of the seasonality, noise intensity, fraction of missing values, disturbance timing, disturbance magnitude, and recovery period. From the simulated time series, we derived a set of recovery metrics using varying pre-processing techniques. Since the introduced disturbance-recovery dynamics be- hind the simulated time series are known, this allowed to (i) evaluate the reliability of the recovery metrics, (ii) evaluate their reliability with respect to the environmental and disturbance parameters, and (iii) gain insight in which pre-processing

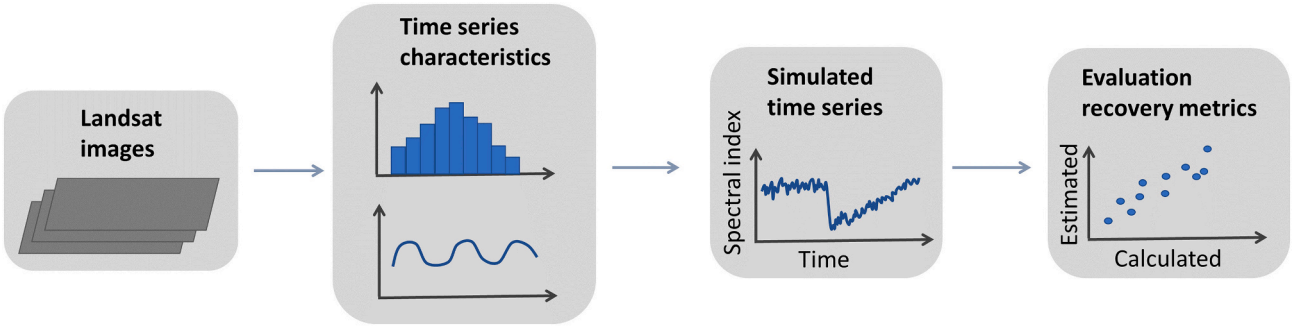

Fig. 1. General overview workflow of the simulation study.

techniques are most suitable to increase their reliability.

2.1. Simulation framework

2.1.1. Components of a simulated time series

Similar to the work of Verbesselt et al. (2010); Lhermitte et al. (2011); De Keersmaecker et al. (2014), optical time series of tropical forest were simulated as the combination of a (i) seasonal, (ii) offset, (iii) remainder and (iv) disturbance component (Eq. (1)).

$$Y(t) = c + S(t) + R(t) + D(t) \quad (1)$$

Where $Y(t)$ equals the simulated time series, c the offset, $S(t)$ the seasonality, $R(t)$ the remainder and $D(t)$ the disturbance component. Seasonality represents an annual cyclic pattern often related to phenology, i.e. the vegetation response to cyclic changes in environmental conditions (Verbesselt et al., 2010). The remainder component relates to residual noise of the time series, e.g. due to remaining aerosols or clouds, but also the short-term vegetation response to environmental conditions (Verbesselt et al., 2016; De Keersmaecker et al., 2014). Finally, the disturbance component is associated with the forest response to a major disturbance (e.g. fire) and its subsequent recovery.

2.1.2. Landsat time series over forest baseline areas

To ensure that the offset, seasonality and remainder components were realistically simulated, the characteristics of the time series components were first extracted from sampled Landsat time series. To that end, $n_c = 1000$ pixels were randomly sampled in undisturbed, intact tropical forest areas. Undisturbed intact tropical forest areas of South America (35°S to 15°N and 30°E to 85°E) were selected. First, forest areas were delineated using the Hansen Global Forest Change (GFC) dataset v1.6 (Hansen et al., 2013). The GFC dataset provides tree canopy cover for the year 2000 and annual tree cover loss. Tree cover is defined as canopy closure for all vegetation taller than 5 m and was derived from Landsat data at 30 m pixel scale (Hansen et al., 2013). In this study, tree cover exceeding a threshold of 80% was used to select dense forest areas. Next, pixels with forest loss were excluded using the forest loss layer of the GFC dataset. The forest loss layer represents stand replacing disturbances, thus implying the conversion of forest to no-forest area. Additionally, non-intact forest areas were excluded using the intact forest layer reported by the World Intact Forest Landscape (IFL) map for 2016 (Potapov et al., 2008). Finally, only pixels that have a probability less than 5% that a fire occurred between 2001 and 2019 were included. These areas were identified using the ESA fire CCI fire dataset (version 5.1), which is based on MODIS spectral and thermal information. The dataset has a pixel size of approximately 250 m and spans the 2001 to 2018 period (Chuvieco et al., 2018).

To characterize the temporal forest dynamics, NBR time series between January 2001 and January 2019 of atmospherically corrected surface reflectance from Landsat 4, 5, 7 and 8 (USGS Tier 1 data) were downloaded from the sampled pixels via the Google Earth Engine (Gorelick et al., 2017). The Landsat data have a pixel size of 30 m and a temporal resolution of 16 days. Quality assurance layers produced by the CFMASK algorithm were used to mask out low quality data related to the presence of clouds, cloud shadows, and snow (Foga et al., 2017).

2.1.3. Characterizing sampled time series

To characterize the offset, seasonality and remainder components, each of the time series were decomposed into a seasonal, trend and remainder component (Fig. 2). Seasonality $S_c(t)$ and the trend $T_c(t)$ component were fitted using a first order harmonic regression and linear trend, respectively. The errors from this model equal the remainder term $R_c(t)$. The following characteristics were then extracted from the decomposed time series: (i) an empirical distribution of seasonal amplitudes, (ii) the seasonal pattern averaged over all pixels located in the Southern hemisphere, (iii) an empirical distribution of the noise magnitude, represented by the standard deviation of the remainder term, (iv) the offset, represented by the mean of the trend component $T_c(t)$ over the n_c pixels, and (v) an empirical distribution of the fraction of missing values.

2.1.4. Simulating time series

Based on the characteristics of these sampled time series, daily, undisturbed time series were simulated with a time span of $n_{ys} = 25$ years. Seasonality was simulated as the average seasonal pattern of the sampled time series that were located in the southern hemisphere, yet rescaled to amplitude A_s. The offset was set to the mean of the trend component $T_c(t)$ over the n_c sampled pixels.

Disturbance-recovery dynamics were subsequently introduced in the simulated time series using a discrete perturbation, i.e. a sudden drop in NBR, followed by (i) a linear recovery, (ii) an exponential decay, or (iii) recovery given by the simple stochastic differential equation (SDE) model $dy = -ry \cdot dt + \sigma \cdot dW$ (Dakos et al., 2012). A layer of additive white noise was added on top of cases (i) and (ii), while case (iii) incorporates the noise automatically via the SDE (more information can be found in Appendix A). The disturbances are defined by the timing (t_d) and magnitude of the abrupt disturbance (D_{mag}), the half time of the subsequent recovery period (t_{rec}) and the noise magnitude (SD_s).

Finally, a fraction of M_s observations are removed randomly from the simulated daily time series to account for missing observations due to the overpass frequency and cloud masking.

In conclusion, the simulation framework allows to simulate time series of disturbed pixels, where the following parameters can be controlled: amplitude of the seasonality (A_s), noise intensity (SD_s), fraction of missing values (M_s), disturbance timing (t_d), disturbance magnitude (D_{mag}), and recovery period (t_{rec}) (Fig. 3).

2.2. Recovery metrics

2.2.1. Forest disturbance dynamics

Three main time periods are used when calculating recovery metrics, i.e. a pre-disturbance, disturbance, and post-disturbance period. These describe the abrupt change in the NBR time series, followed by a gradual

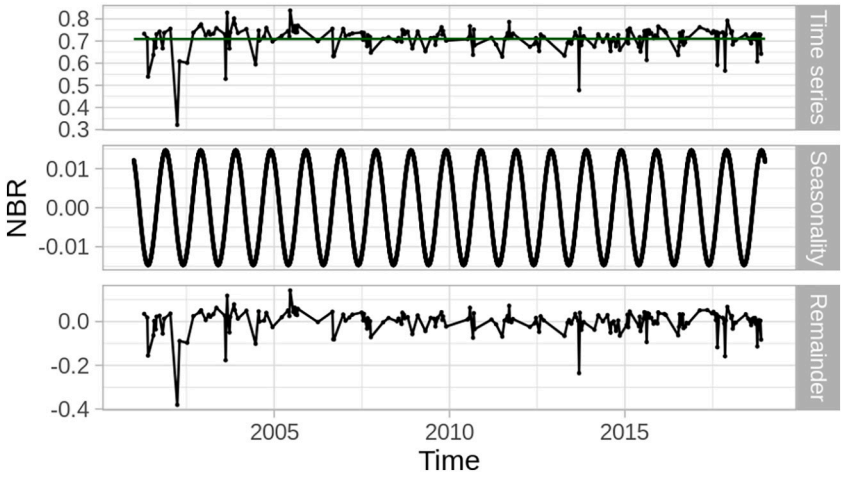

Fig. 2. Example of a decomposed time series: a time series with trend component (green) (top), seasonal component (middle), and remainder component (bottom). (For interpretation of the references to colour in this figure legend, the reader is referred to the web version of this article.)

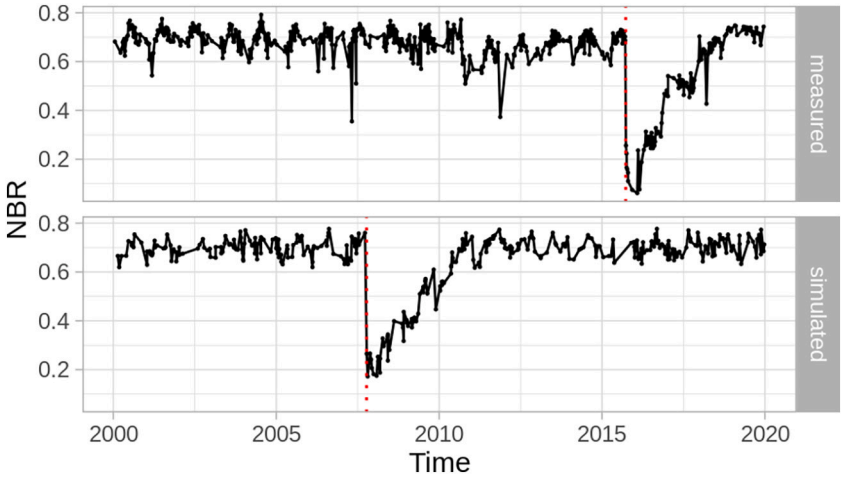

Fig. 3. Example of a sampled and simulated NBR time series with abrupt (fire) perturbations (red dotted lines). The simulated time series has a high seasonality amplitude, low noise magnitude, and low fraction of missing values. Its disturbance has a magnitude of 0.5 and takes place in 2007, followed by a linear recovery with a half time of 1.5 years. (For interpretation of the references to colour in this figure legend, the reader is referred to the web version of this article.)

recovery period (Fig. 4). First, the pre-disturbance period t_{pre} spans n_{pre} years before the disturbance to the start of the disturbance. NBR values during this period define the pre-disturbance condition of the forest, and are considered to be a reference. Pixels that reach these NBR values again after the disturbance are considered to be spectrally recovered. Second, the disturbance period t_{dist} covers n_{dist} years, starting from the time of disturbance. NBR values during this period characterize the forest condition during the disturbance. Hence, the NBR change from the pre-disturbance to the disturbance period describes the disturbance magnitude, which is assumed to be related to the severity of the disturbance impact. Finally, the post-disturbance periods t_{post} and t_{Δ}, start $n^{start}{}_{post}$ *and* $n^{start}{}_{\Delta}$ years after the disturbance and span n_{post} and n_{Δ} years, respectively. This period provides information about the forest condition after the disturbance. The change in mean NBR between the disturbance and post-disturbance period relates to the recovery magnitude.

2.2.2. Recovery metrics

We evaluated three complementary recovery metrics: the Relative Recovery Index (RRI), the Ratio of Eighty Percent (R80P), and Year on Year Average (YrYr) (Fig. 5). First, the RRI equals the recovery magnitude relative to the disturbance magnitude (Kennedy et al., 2012; Frazier et al., 2018). A RRI value of zero indicates that no recovery has taken place, while a value of one denotes that the change in the response variable due to the disturbance has been compensated n years after the disturbance. The ability of the RRI to include the disturbance magnitude is specific to the RRI, and is particularly interesting as it allows to account for the intensity or impact that the disturbance had (Frazier et al., 2018). Second, the R80P metric measures to what extent the time series has reached 80% of its pre-disturbance value (Pickell et al., 2016; Frazier et al., 2018). A R80P value of one means that 80% of the pre-disturbance value has been reached n years after the disturbance. Values lower/higher than one indicate that less/more than 80% has been reached. Note that, in contrast to the other metrics, the R80p is sensitive to the absolute values of the pre- and post-disturbance state. A shift of the NBR time series values would thus affect the R80p. Third, the YrYr metric is related to the recovery rate over a fixed time interval after the disturbance (Frazier et al., 2018). Positive YrYr values indicate a positive trend after the disturbance, while a zero value suggests that – over the evaluated post-disturbance period – no recovery of the remotely sensed response variable occurred. In contrast to the RRI and R80P, this metric is not directly related to the disturbance magnitude or the pre-disturbance values.

The RRI, R80P and YrYr metrics are typically derived from yearly

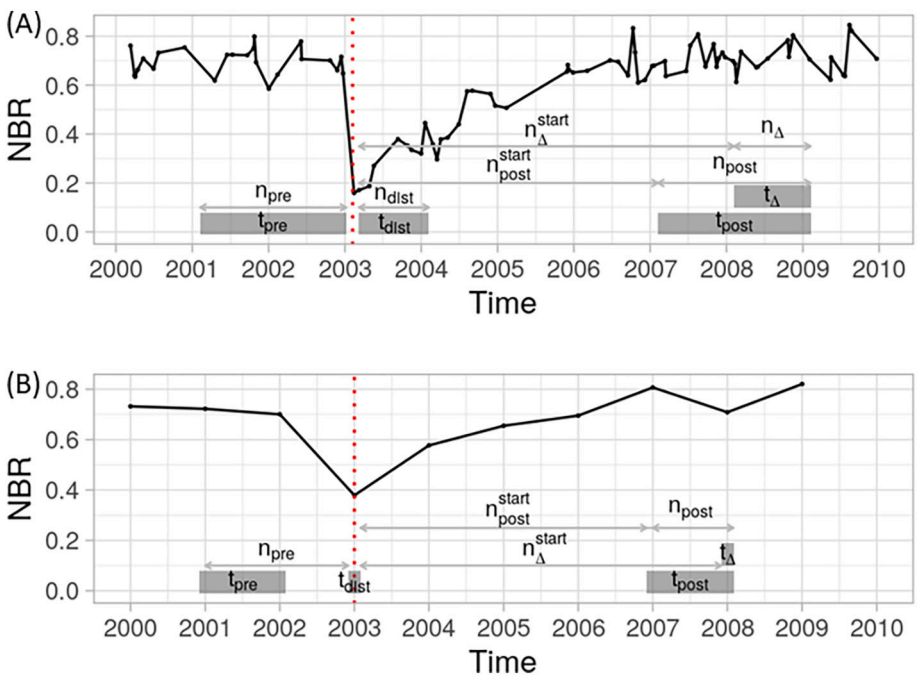

Fig. 4. Illustration of the pre-disturbance, disturbance and post-disturbance measurement periods for (a) sub-annual and (b) annual time series. Here, the pre-disturbance measurement period (t_{pre}) spans n_{pre} = 2 years, the disturbance measurement period (t_{dist}) spans n_{dist} = 1 year, the post-disturbance measurement period (t_{post}) spans n_{post} = 2 years and starts n^{start}_{post} = 4 years after the start of the disturbance. Finally, the post-disturbance measurement period (t_{Δ}) spans n_{Δ} = 1 year and starts n^{start}_{Δ} = 5 years after the start of the disturbance. The red dotted line indicates the timing of the disturbance. (For interpretation of the references to colour in this figure legend, the reader is referred to the web version of this article.)

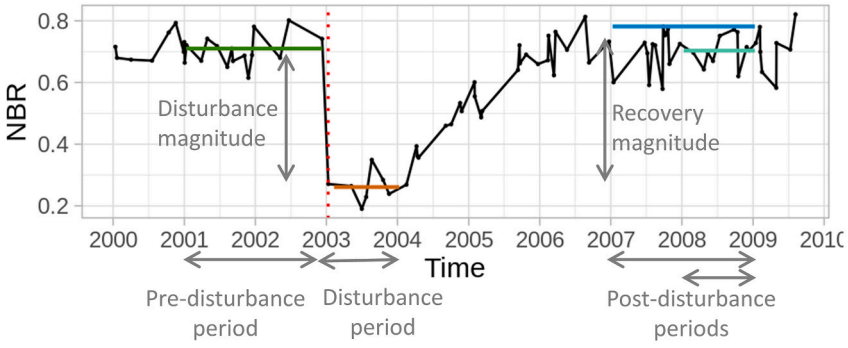

Recovery indicator	Equation	Explanation
Relative Recovery Index	$RRI = \frac{\lvert \max(f(t_{post})) - \bar{f}(t_{dist}) \rvert}{\lvert \bar{f}(t_{pre}) - \bar{f}(t_{dist}) \rvert}$	Recovery magnitude relative to disturbance magnitude
Ratio of Eighty Percent	$R80p = \frac{\max(f(t_{post}))}{0.8\,\bar{f}(t_{pre})}$	Post-disturbance state relative to 80% of pre-disturbance state
Year on Year Average	$YrYr = \frac{\bar{f}(t_{\Delta}) - \bar{f}(t_{dist})}{\bar{t}_{\Delta} - \bar{t}_{dist}}$	Related to post-disturbance slope

Fig. 5. Equations of the three evaluated recovery metrics. $f(t_{pre})$, $f(t_{dist})$, $f(t_{post})$, and $f(t_{\Delta})$ stand for the NBR values over the pre-disturbance, disturbance, post-disturbance, and YrYr specific post-disturbance measurement period, respectively. The red dotted line in the figure stands for the timing of the disturbance. (For interpretation of the references to colour in this figure legend, the reader is referred to the web version of this article.)

best available pixel Landsat time series (Pickell et al., 2016; Frazier et al., 2018; White et al., 2017), which cover a relatively long time span. Given the short time span of recently launched sensors like the Sentinels, we also aimed to test the performance of recovery metrics when the data covers a short time span and hence a short post-recovery period is available. To this end, we modified the recovery metrics by making the time period to measure the pre-disturbance, disturbance, and post-disturbance condition flexible.

2.3. Evaluating pre-processing techniques

We calculated the recovery metrics using different time series pre-processing techniques and recovery metric settings to evaluate their impact on the reliability of the metrics. First, temporal aggregation of time series from dense, to quarterly means and annual values was tested. Annual observations were derived by taking the observation closest to the seasonal maximum, with a maximum time difference of one month.

Second, we tested the effect of noise reduction techniques by

calculating the recovery metrics on (i) raw time series, (ii) after smoothing using a rolling mean with window size of one year, and (iii) after performing time series segmentation (Fig. 6). The time series segmentation detects breaks in a linear regression model that consists of a trend and harmonic term. More information about the method can be found in Zeileis et al. (2010). The rolling mean and time series segmentation reduce the presence short-term fluctuations and extract the overall change patterns. As such, the influence of white noise on the extracted recovery metrics is expected to be minimized.

Third, the effect of the length of the post-disturbance measurement period was assessed. The performance of the recovery metrics was tested using a long and short recovery measurement period (Table 1). The long recovery measurement period (ca 5 years after disturbance) aligns with the definition of the recovery metrics in (Frazier et al., 2018). The short period (ca 1 year after disturbance) is relevant for short time series, such as those obtained from the Sentinels.

2.4. Set-up sensitivity analysis and reliability measures

Using the simulation framework, the sensitivity of the recovery metrics to single environmental and disturbance parameters was evaluated. As such, time series were simulated over increasing values for each of these parameters (i.e. very low, low, medium, and high evaluated values in Table 2). While evaluating the effect of one parameter, the other parameters were fixed (i.e. set to fixed value range in Table 2). For the environmental parameters, the evaluated values were defined by the quantiles of sampled pixel parameters. For the disturbance parameters, the categories were set to reasonable values for tropical forests. We however extended the values of the recovery time parameter beyond the expected range to be representative for other forest types as well.

For each of the evaluated values 10,000 time series were simulated and recovery metrics de- rived. As the introduced disturbance-recovery signal is exactly known, this simulation framework allows to compare the true recovery metrics with those measured from the simulated data. Hence, their performance was quantified using the RMSE and R^2.

Table 1
The characteristics of the pre-disturbance, disturbance and post-disturbance time periods used to derive the recovery metrics. The values are given for two set-ups: (i) a short and (ii) a long post-disturbance measurement period.

Name	Values [years]	
	Short	Long
n_{pre}	2	2
n_{dist}	1	1
n_{post}^{start}	1	4
n_{post}	1	2
n_{Δ}^{start}	1	5
n_{Δ}	1	1

3. Results

3.1. Reliability of recovery metrics

Our comparison of the reliability of each recovery metric (Fig. 7) indicates that the RRI is the most difficult metric to estimate accurately. The two other recovery metrics, i.e. the R80p and YrYr, perform approximately equally well.

3.2. Effect of environmental and disturbance characteristics

The average error introduced on the recovery metrics for increasing levels of each environmental and disturbance parameter (Fig. 8) provides insight in the sensitivity of the recovery metrics. First, increasing fraction of missing values and an increasing noise level increased the error, while the seasonal amplitude has nearly no effect. These trends are the same for all three recovery metrics. Second, increasing levels of the disturbance parameters, i.e. disturbance magnitude, disturbance timing, and recovery period, generally tend to decrease the error. Overall, the disturbance parameters show a similar magnitude of impact on the error. Yet, the impact of very low disturbance magnitude and disturbance timing values is more important than the impact of a very low recovery period for the RRI. This effect can not be observed for the other recovery metrics.

It is important to note that the error on the recovery metrics can become relatively high. For example, the RMSE of the RRI can reach

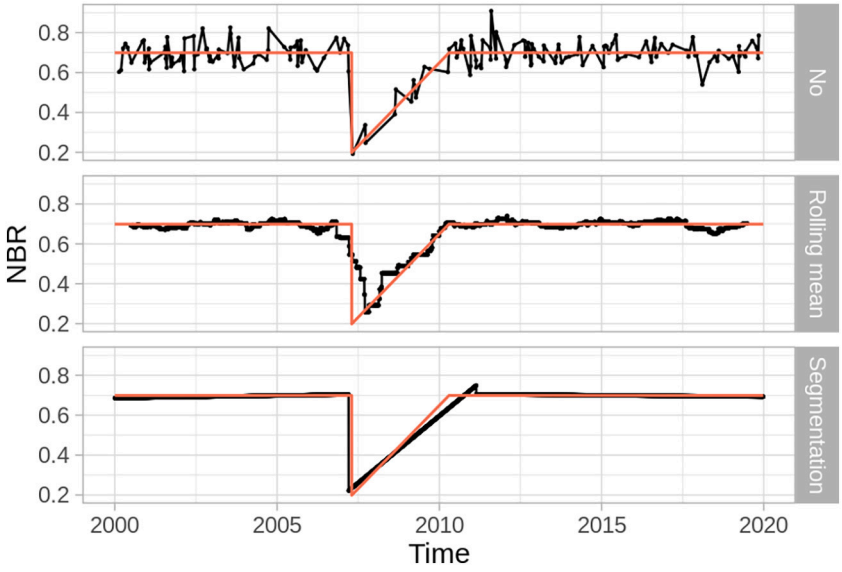

Fig. 6. Illustration of the evaluated noise removal techniques: a simulated time series with no noise removal technique (top), rolling mean filter (middle), and segmentation (bottom). The red line shows the simulated reference disturbance-recovery dynamic (i.e. ground truth). (For interpretation of the references to colour in this figure legend, the reader is referred to the web version of this article.)

Table 2
Simulation set-up: values for each environmental (noise intensity SD_s, seasonal amplitude A_s, fraction missing values M_s) and disturbance parameter (disturbance magnitude D_{mag}, recovery half time t_{rec} [year], and disturbance time t_d [year]) that are used for simulating time series.

Parameter		Evaluated values				Fixed
		Very low	Low	Medium	High	Medium
			Q 5–25%	Q 40–60%	Q 75–95%	Q 40–60%
Environmental	*SDs*	0	0.032–0.042	0.048–0.054	0.061–0.097	0.048–0.054
	As	0	0.006–0.014	0.018–0.025	0.030–0.044	0.018–0.025
	Ms	0.938	0.954–0.969	0.974–0.980	0.984–0.993	0.974–0.980
Disturbance	*Dmag*	0.05–0.15	0.15–0.25	0.25–0.35	0.35–0.45	0.25–0.35
	trec	0.5–1	1.5–2	2.5–3	3.5–4	2.5–3
	td	3–5	7–9	11–13	15–17	11–13

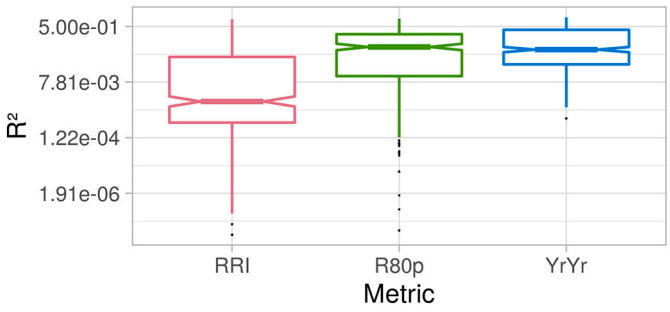

Fig. 7. Boxplots of the reliability (R^2) of each recovery metric using all preprocessing methods, time series simulation parameters, and recovery measurement periods. Only results of time series with a linear recovery are shown. The y axis was log transformed to enhance the comparison. The black dots show the extreme observations (i.e. falling outside boxplot whiskers).

error values around 16. This means that the error would be 16 times the true value for a pixel that is fully recovered.

3.3. Effect of preprocessing techniques

To evaluate the effect of preprocessing techniques on the accuracy of the recovery metrics, three processing options were tested: (i) aggregation the temporal resolution of the data from dense time series to quarterly and annual values, (ii) noise removal techniques like using a rolling mean filter and time series segmentation, and (iii) comparing recovery metrics that use a short (1 year) and long (ca 5 years) recovery measurement period (Fig. 9).

This leads to three main findings. First, overall no temporal aggregation results in a smaller error on the recovery metrics as compared to temporal aggregation to quarterly or annual temporal resolution. Second, the error generally tends to increase from the use of time series segmentation to the use of a rolling mean smoothing filter and using no noise removal technique. In contrast, the variability of the error after segmentation is often larger than the other methods. Third, the effect of using a short versus long post disturbance measurement period is minimal. These trends are consistent among all three recovery metrics.

4. Discussion

4.1. Reliability of recovery metrics

The R80p and the YrYr metric perform equally well, while the RRI showed to be the least reliable recovery metric. The RRI metric equals the fraction of the recovery magnitude and the disturbance magnitude (Frazier et al., 2018). This implies that for very small disturbance magnitudes, the RRI values may become very large, potentially explaining its lower reliability. The importance of the RRI to accurately measure the recovery magnitude is also reflected by its sensitivity to disturbance characteristics: the impact of the disturbance magnitude and disturbance timing is more important for the RRI than the other recovery metrics. On top of that, both the RRI and the R80p use maximum values over the post-disturbance measurement period to represent the post-disturbance state. The dependency of the metric on single observations could additionally decrease their reliability. Yet, although it is important to take into account the reliability of the metrics, the three metrics provide complementary information (Frazier et al., 2018). Selecting a single metric to study recovery capacity may thus be too limiting given the objective of any specific recovery study.

4.2. Effect of environmental and disturbance characteristics

Comparing the effect of the environmental parameters indicates that the number of missing values and noise level have the largest impact on the reliability of recovery metrics in tropical forest, while seasonal amplitude has nearly no effect. This could be expected since the disturbance periods span entire years, thus averaging out seasonal effects. Moreover, seasonal amplitude in tropical forest is minor, while the noise levels and missing values are significant due to persistent cloud coverage (De Keersmaecker et al., 2014). This is in contrast with for instance temperate or dry forests, where seasonal NBR patterns are more pronounced, or dryland dynamics, where the interannual variability due to e.g. water availability is substantial. It could thus be expected that challenges and solutions to assess recovery capacity are partly ecosystem specific. For instance, in Mediterranean-type ecosystems, normalization between fire and no-fire plots have shown to successfully reduce the impact of climate-driven interannual variability and thus increase the reliability of recovery metrics (Storey et al., 2016). Finally, the impact of missing values and the noise level underlines the importance of high quality time series data for recovery studies, i.e. a small noise level and as low as possible number of missing data. Hence, initiatives to combine data from different sensors are very interesting as they may reduce the number of missing data.

4.3. Effect of pre-processing techniques

To get insight in the most optimal implementation of the recovery metrics, three effects were tested: (i) the use of temporal aggregation, (ii) the use of a noise removal techniques, and (iii) the use of a long versus short post-disturbance period.

Comparing the reliability of the recovery metrics for varying levels of temporal aggregation indicated that the use of daily time series performed better than the quarterly or annual aggregated ones. Since the overpass frequency of Landsat is much lower (Wulder et al., 2012), this approach results in a large number of missing values. In addition, the advantage of an improved reliability may be counterbalanced by an increase in data volumes and processing time. Hence, one could expect that temporal aggregation to bimonthly or monthly values would be an interesting middle ground.

The high dependency of the recovery metrics on the noise level suggests that pre-preprocessing methods that aim to remove noise would significantly increase the reliability of the recovery metrics. Indeed, the

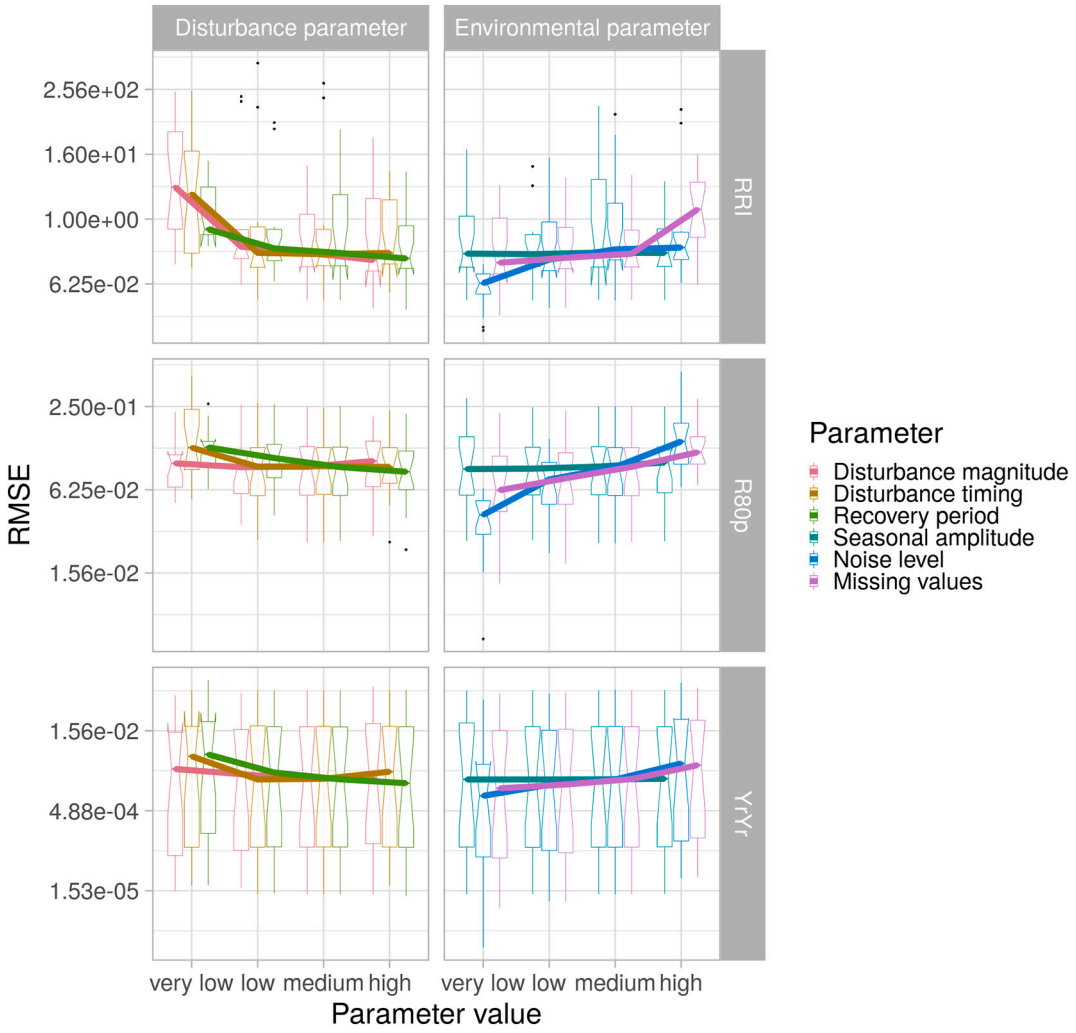

Fig. 8. Boxplots of the reliability (RMSE) of each recovery metric (rows) against categories of disturbance (left column) and environmental (right column) parameters. Only results of time series with a linear recovery are shown. The y axis was log transformed to enhance the comparison. Please note that a comparison of RMSE values between recovery metrics is not meaningful since the recovery metrics have different scales and value ranges.

use of time series segmentation and a rolling mean filter on dense time series overall resulted in recovery metrics with a higher reliability compared to the use of no noise removal technique. While on average the time series segmentation showed an higher reliability compared to the rolling mean filter, the error on the recovery metrics was often also more variable.

Time series segmentation is expected to better handle sharp transitions (i.e. due to the disturbance) as compared to a rolling mean filter. A rolling mean filter may however better pick up non-linear recovery patterns as compared to time series segmentation, since the latter considers linear changes (Verbesselt et al., 2010). As such, assuming linear recovery patterns in the simulation set-up could potentially favour the time series segmentation. To evaluate the effect of this assumption, the analysis was repeated while simulating non-linear recovery patterns (i.e. exponential and SDE; see appendix B). This showed that time series segmentation outperforms the other noise removal techniques for both linear and exponential recovery patterns, indicating that the assumption of linearity has a minor impact. All methods however perform equally well for the recovery pattern given by a SDE. This is likely related to different noise patterns. The time series with linear and exponential recovery patterns are simulated with uncorrelated noise, while the series with a recovery given by a SDE have autocorrelated noise.

Although time series segmentation on dense time series performs on average equally or better than the other approaches, the variability of the errors of the recovery metrics is also higher. It is thus important to note that its reliability strongly decreases in three cases: (i) small disturbance magnitudes, (ii) very short recovery periods, and (iii) disturbances that take place towards the edge of the time series (as shown in appendix C). This has several implications for its usage. For instance, the reduced performance of recovery metrics for minor disturbances could be avoided by calculating the metrics only for medium to large disturbances. This approach was for example also followed in the work of Frazier et al. (2018) over boreal forests, where a threshold on the drop in NBR was applied to select fires with medium to high severity. Next, the decreased reliability of time series segmentation for fast recovery rates might be related to the use of a fixed *h* factor in this study. The *h* factor represents the minimal segment size that can be detected (Verbesselt et al., 2010). For fast recovery rates, the post-disturbance (i.e. recovery) segment could become smaller than detectable by the *h* factor.

Finally, to evaluate the performance of the recovery metrics for short time series, the recovery metrics were also implemented using a short post-disturbance measurement period and the effect of the disturbance position towards the time series edge was evaluated. Similar to findings of Senf et al. (2019), where a period of 3, 10 or 15 years was evaluated in central Europe, the use of a short versus long post-disturbance measurement period had nearly no effect on the reliability of the recovery metrics. However, disturbances that take place towards the time series edge showed a high impact on the performance of the time series

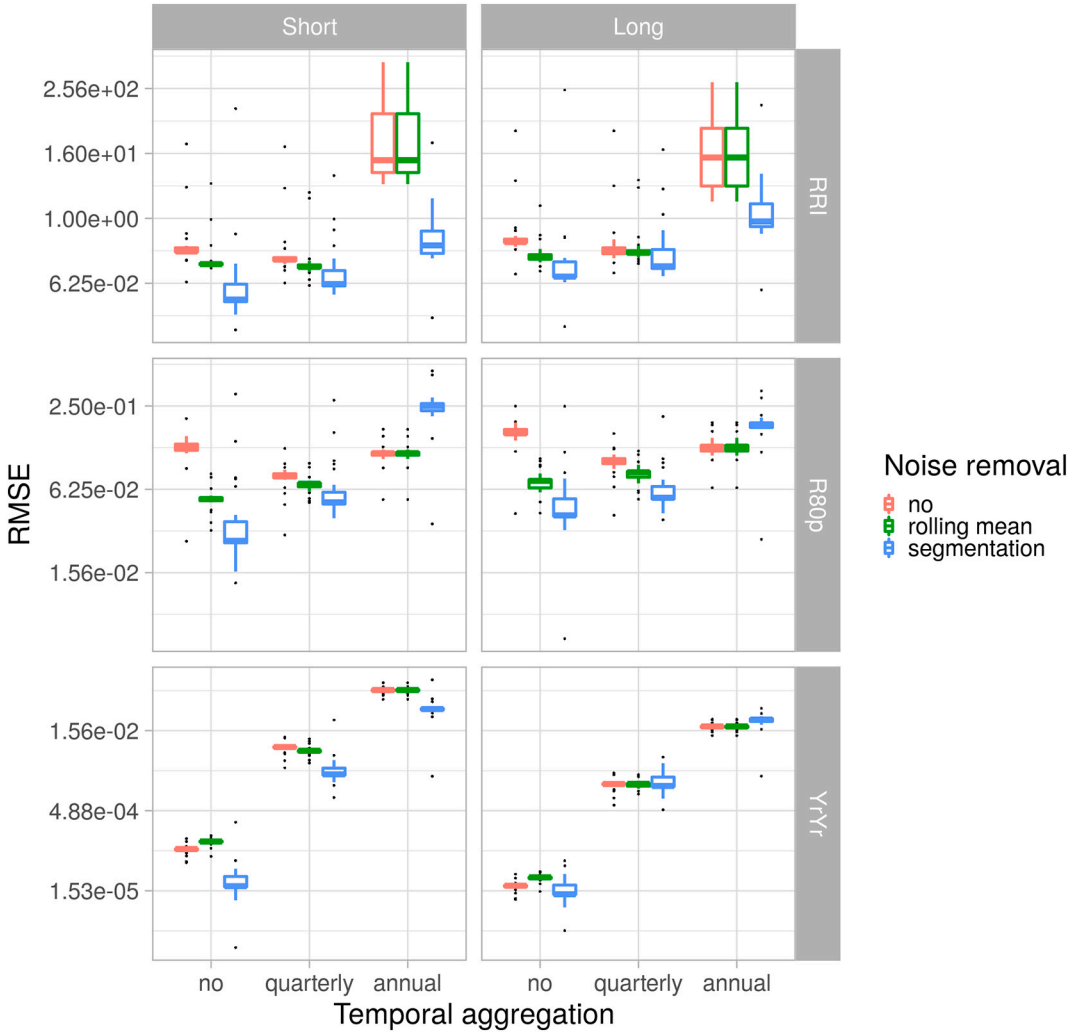

Fig. 9. Boxplots of the reliability (RMSE) of each recovery metric (rows) for varying levels of temporal aggregation (x axis), noise removal techniques (colors), and the use of a short and long post recovery period (columns). Only results of time series with a linear recovery are shown. The y axis was log transformed to enhance the comparison. Please note that a comparison of RMSE values between recovery metrics is not meaningful since the recovery metrics have different scales and value ranges.

segmentation. The latter could limit its usability for very short time series. This problem is particularly important when using only recently launched sensors (e.g. Sentinels) and may be reduced when time series are getting longer. Using longer time series (e.g. Landsat (Wulder et al., 2012)) or harmonized products, such as the harmonized Landsat Sentinel product (Claverie et al., 2018), may overcome this challenge.

4.4. *Limitations and advantages of the simulation framework*

The use of a simulation framework has several advantages (Awty-Carroll et al., 2019). First, there is no need to gather ground truth data on forest recovery capacity, which are hard to obtain over tropical forest. Second, it can provide insights in the sensitivity of the recovery metrics (Verbesselt et al., 2010; Lhermitte et al., 2011). For example, it is possible to evaluate the effect of single data characteristics (e.g. noise level or disturbance timing) and (pre-)processing techniques on the reliability of the recovery metrics. Third, we demonstrated this approach for abrupt disturbances in tropical forests and the results shown here are thus only applicable to this ecosystem, type of disturbance, area of interest, and satellite data. For example, the use of a step function to simulate a disturbance is considered to represent the forest response to an abrupt disturbance (e.g. forest fire or logging), but may not be representative for slower disturbance dynamics (e.g. droughts, diseases) (Awty-Carroll et al., 2019). Yet, the general framework could be transferred to other study areas, ecosystems, or datasets (e.g. Sentinels) and thus serve as a test bed for other researchers. This is enhanced by making the code freely available (see De Keersmaecker and Rodr'ıguez-Sanchez, 2020 for the link). Applying the simulation framework on another dataset would require to first sample time series. Sampling time series is needed to characterize a realistic range of the environmental parameter values. Next, the settings of the recovery metrics that need to be tested should be defined (e.g. length of the pre-disturbance, disturbance and post-disturbance period). Finally, realistic levels of the disturbance parameters should be defined. Applying the framework to other disturbance types or other ecosystems than tropical forest might require some additional modifications, such as introducing interannual variability in the simulated time series.

Despite the advantages of using a simulation framework to explore the sensitivity of recovery metrics, it is important to acknowledge that validation using field observations is indispensable. Notwithstanding our efforts to realistically simulate time series, it remains challenging to fully cover the complexity of measured data using a simulation analysis. Moreover, a validation with field observations can give additional insights on the extent to which the remotely sensed recovery metrics relate to attributes observed in the field such as tree height (White et al., 2019).

4.5. Outlook

In this study, the effects of environmental and disturbance characteristics were tested for recovery metrics derived from Landsat time series. Yet, the simulation framework could also be used to evaluate recovery metrics derived from new or recently developed datasets, such as Sentinel-2 or Harmonized Landsat Sentinel datasets. In addition to optical data, other data sources could be tested, such as RADAR data. Moreover, the simulation framework could be extended to test other characteristics of interest. For instance, effects of multiple sequential disturbances or interannual variability could be tested. The latter is expected to be especially relevant for forest in dryland areas.

Finally, the launch of new satellite missions opens opportunities to gain insight in the per- formance and sensitivity of the optical recovery metrics to assess changes in forest biomass and structure. For example, the recently launched Global Ecosystem Dynamics Investigation (GEDI) mission and future ESA Biomass mission will provide data related to forest canopy height, structure, and biomass (Dubayah et al., 2020; Carreiras et al., 2017). Moreover, the ESA Biomass mission is expected to greatly improve forest biomass monitoring in the tropics, and hence also forest recovery assessment, which is critical given the great knowledge gaps and needs (Carreiras et al., 2017; Herold et al., 2019).

Funding

This work was supported by the Netherlands eScience Center under file number ASDI.2018.068 (project RETURN).

CRediT authorship contribution statement

Wanda De Keersmaecker: Conceptualization, Methodology, Software, Writing – original draft. **Pablo Rodríguez-Sánchez:** Methodology, Software, Writing – review & editing. **Milutin Milenković:** Methodology, Writing – review & editing. **Martin Herold:** Writing – review & editing, Supervision. **Johannes Reiche:** Methodology, Writing – review & editing, Supervision. **Jan Verbesselt:** Conceptualization, Methodology, Writing – review & editing, Supervision.

Declaration of Competing Interest

The authors declare that they have no known competing financial interests or personal relationships that could have appeared to influence the work reported in this paper.

Acknowledgements

We would like to acknowledge and thank for the granted access to the Spider high-throughput platform and the support provided by SURFsara. We also would like to thank the anonymous reviewers for their valuable comments and suggestions that greatly improved our manuscript.

Appendix A. Supplementary data

Supplementary data to this article can be found online at https://doi.org/10.1016/j.rse.2022.112991.

References

Abel, C., Horion, S., Tagesson, T., Brandt, M., Fensholt, R., 2019. Towards improved remote sensing based monitoring of dryland ecosystem functioning using sequential linear regression slopes (sergs). Remote Sens. Environ. 224, 317–332.
Alencar, A.A., Brando, P.M., Asner, G.P., Putz, F.E., 2015. Landscape fragmentation, severe drought, and the new amazon forest fire regime. Ecol. Appl. 25, 1493–1505.
Aragao, L.E., Shimabukuro, Y.E., 2010. The incidence of fire in amazonian forests with implications for redd. Science 328, 1275–1278.
Aragao, L.E., Anderson, L.O., Fonseca, M.G., Rosan, T.M., Vedovato, L.B., Wagner, F.H., Silva, C.V., Junior, C.H.S., Arai, E., Aguiar, A.P., et al., 2018. 21st century drought-related fires counteract the decline of amazon deforestation carbon emissions. Nat. Commun. 9, 1–12.
Awty-Carroll, K., Bunting, P., Hardy, A., Bell, G., 2019. An evaluation and comparison of four dense time series change detection methods using simulated data. Remote Sens. 11, 2779.
Brando, P., Macedo, M., Silv'erio, D., Rattis, L., Paolucci, L., Alencar, A., Coe, M., Amorim, C., 2020. Amazon Wildfires: Scenes from a Foreseeable Disaster, Flora, p. 151609.
Carreiras, J.M., Quegan, S., Le Toan, T., Minh, D.H.T., Saatchi, S.S., Carvalhais, N., Reichstein, M., Scipal, K., 2017. Coverage of high biomass forests by the esa biomass mission under defense restrictions. Remote Sens. Environ. 196, 154–162.
Chuvieco, E., Lizundia-Loiola, J., Pettinari, M.L., Ramo, R., Padilla, M., Tansey, K., Mouil-Lot, F., Laurent, P., Storm, T., Heil, A., et al., 2018. Generation and analysis of a new global burned area product based on modis 250 m reflectance bands and thermal anomalies. Earth Syst. Sci. Data 10, 2015–2031.
Claverie, M., Ju, J., Masek, J.G., Dungan, J.L., Vermote, E.F., Roger, J.-C., Skakun, S.V., Justice, C., 2018. The harmonized landsat and sentinel-2 surface reflectance data set. Remote Sens. Environ. 219, 145–161.
Dakos, V., Carpenter, S.R., Brock, W.A., Ellison, A.M., Guttal, V., Ives, A.R., Kefi, S., Livina, V., Seekell, D.A., van Nes, E.H., et al., 2012. Methods for detecting early warnings of critical transitions in time series illustrated using simulated ecological data. PLoS One 7, e41010.
De Keersmaecker, W., Rodr'iguez-Sanchez, P., 2020. RETURN-project/BenchmarkRecovery: Benchmarking Recovery Metrics Derived from Remote Sensing Time Series. URL:
De Keersmaecker, W., Lhermitte, S., Honnay, O., Farifteh, J., Somers, B., Coppin, P., 2014. How to measure ecosystem stability? An evaluation of the reliability of stability metrics based on remote sensing time series across the major global ecosystems. Glob. Chang. Biol. 20, 2149–2161.
Drusch, M., Del Bello, U., Carlier, S., Colin, O., Fernandez, V., Gascon, F., Hoersch, B., Isola, C., Laberinti, P., Martimort, P., et al., 2012. Sentinel-2: Esa's optical high-resolution mission for gmes operational services. Remote Sens. Environ. 120, 25–36.
Dubayah, R., Blair, J.B., Goetz, S., Fatoyinbo, L., Hansen, M., Healey, S., Hofton, M., Hurtt, G., Kellner, J., Luthcke, S., et al., 2020. The global ecosystem dynamics investigation: high-resolution laser ranging of the earth's forests and topography. Sci. Remote Sens. 1, 100002.
Durigan, G., Ratter, J.A., 2016. The need for a consistent fire policy for cerrado conservation. J. Appl. Ecol. 53, 11–15.
Fidelis, A., Alvarado, S.T., Barradas, A.C.S., Pivello, V.R., 2018. The year 2017: megafires and management in the cerrado. Fire 1, 49.
Flores, B.M., Holmgren, M., Xu, C., Van Nes, E.H., Jakovac, C.C., Mesquita, R.C., Scheffer, M., 2017. Floodplains as an achilles' heel of amazonian forest resilience. Proc. Natl. Acad. Sci. 114, 4442–4446.
Foga, S., Scaramuzza, P.L., Guo, S., Zhu, Z., Dilley Jr., R.D., Beckmann, T., Schmidt, G.L., Dwyer, J.L., Hughes, M.J., Laue, B., 2017. Cloud detection algorithm comparison and validation for operational landsat data products. Remote Sens. Environ. 194, 379–390.
Frazier, R.J., Coops, N.C., Wulder, M.A., 2015. Boreal shield forest disturbance and recovery trends using landsat time series. Remote Sens. Environ. 170, 317–327.
Frazier, R.J., Coops, N.C., Wulder, M.A., Hermosilla, T., White, J.C., 2018. Analyzing spatial and temporal variability in short-term rates of post-fire vegetation return from landsat time series. Remote Sens. Environ. 205, 32–45.
Gorelick, N., Hancher, M., Dixon, M., Ilyushchenko, S., Thau, D., Moore, R., 2017. Google earth engine: planetary-scale geospatial analysis for everyone. Remote Sens. Environ. 202, 18–27.
Hansen, M.C., Potapov, P.V., Moore, R., Hancher, M., Turubanova, S.A., Tyukavina, A., Thau, D., Stehman, S., Goetz, S.J., Loveland, T.R., et al., 2013. High-resolution global maps of 21st-century forest cover change. science 342, 850–853.
Hansen, M.C., Wang, L., Song, X.-P., Tyukavina, A., Turubanova, S., Potapov, P.V., Stehman, S.V., 2020. The fate of tropical forest fragments. Sci. Adv. 6, eaax8574.
Herold, M., Carter, S., Avitabile, V., Espejo, A.B., Jonckheere, I., Lucas, R., McRoberts, R. E., Næsset, E., Nightingale, J., Petersen, R., et al., 2019. The role and need for space-based for- Est biomass-related measurements in environmental management and policy. Surv. Geophys. 40, 757–778.
Hirota, M., Holmgren, M., Van Nes, E.H., Scheffer, M., 2011. Global resilience of tropical forest and savanna to critical transitions. Science 334, 232–235.
Hislop, S., Jones, S., Soto-Berelov, M., Skidmore, A., Haywood, A., Nguyen, T.H., 2018. Using landsat spectral indices in time-series to assess wildfire disturbance and recovery. Remote Sens. 10, 460.
Kelly, L., Brotons, L., 2017. Using fire to promote biodiversity. Science 355, 1264–1265.
Kennedy, R.E., Yang, Z., Cohen, W.B., 2010. Detecting trends in forest disturbance and recovery using yearly landsat time series: 1. Landtrendr—temporal segmentation algorithms. Remote Sens. Environ. 114, 2897–2910.
Kennedy, R.E., Yang, Z., Cohen, W.B., Pfaff, E., Braaten, J., Nelson, P., 2012. Spatial and temporal patterns of forest disturbance and regrowth within the area of the northwest forest plan. Remote Sens. Environ. 122, 117–133.
Key, C., 2006. Landscape assessment (LA): sampling and analysis methods. In 'FIREMON: fire effects monitoring and inventory system'. In: Lutes, D.C., Keane, R.E., Caratti, J. F., Key, C.H., Benson, N.C., Sutherland, S., Gangi, L.J. (Eds.), USDA Forest Service, Rocky Mountain Research Station, Technical Report, General Technical Report RMRS-GTR-164, pp. LA1–LA51 (Fort Collins, CO).
Lhermitte, S., Verbesselt, J., Verstraeten, W.W., Coppin, P., 2011. A comparison of time series similarity measures for classification and change detection of ecosystem dynamics. Remote Sens. Environ. 115, 3129–3152.

Nguyen, T.H., Jones, S.D., Soto-Berelov, M., Haywood, A., Hislop, S., 2018. A spatial and temporal analysis of forest dynamics using landsat time-series. Remote Sens. Environ. 217, 461–475.
Pettorelli, N., Laurance, W.F., O'Brien, T.G., Wegmann, M., Nagendra, H., Turner, W., 2014. Satellite remote sensing for applied ecologists: opportunities and challenges. J. Appl. Ecol. 51, 839–848.
Pickell, P.D., Hermosilla, T., Frazier, R.J., Coops, N.C., Wulder, M.A., 2016. Forest recovery trends derived from landsat time series for north american boreal forests. Int. J. Remote Sens. 37, 138–149.
Potapov, P., Yaroshenko, A., Turubanova, S., Dubinin, M., Laestadius, L., Thies, C., Aksenov, D., Egorov, A., Yesipova, Y., Glushkov, I., et al., 2008. Mapping the world's intact forest landscapes by remote sensing. Ecol. Soc. 13.
Schmidt, I.B., Moura, L.C., Ferreira, M.C., Eloy, L., Sampaio, A.B., Dias, P.A., Berlinck, C. N., 2018. Fire management in the brazilian savanna: first steps and the way forward. J. Appl. Ecol. 55, 2094–2101.
Senf, C., Muller, J., Seidl, R., 2019. Post-disturbance recovery of forest cover and tree height differ with management in central europe. Landsc. Ecol. 34, 2837–2850.
Silva Junior, C.H., Aragao, L.E., Fonseca, M.G., Almeida, C.T., Vedovato, L.B., Anderson, L.O., 2018. Deforestation-induced fragmentation increases forest fire occurrence in central brazilian Amazonia. Forests 9, 305.
Silva Junior, C.H., Anderson, L.O., Silva, A.L., Almeida, C.T., Dalagnol, R., Pletsch, M.A., Penha, T.V., Paloschi, R.A., Aragao, L.E., 2019. Fire responses to the 2010 and 2015/2016 amazonian droughts. Front. Earth Sci. 7, 97.
Staal, A., Tuinenburg, O.A., Bosmans, J.H., Holmgren, M., van Nes, E.H., Scheffer, M., Zemp, D.C., Dekker, S.C., 2018. Forest-rainfall cascades buffer against drought across the amazon. Nat. Clim. Chang. 8, 539.
Storey, E.A., Stow, D.A., O'Leary, J.F., 2016. Assessing postfire recovery of chamise chaparral using multi-temporal spectral vegetation index trajectories derived from landsat imagery. Remote Sens. Environ. 183, 53–64.
Taubert, F., Fischer, R., Groeneveld, J., Lehmann, S., Muller, M.S., Rodig, E., Wiegand, T., Huth, A., 2018. Global patterns of tropical forest fragmentation. Nature 554, 519–522.
Torres, R., Snoeij, P., Geudtner, D., Bibby, D., Davidson, M., Attema, E., Potin, P., Rommen, B., Floury, N., Brown, M., et al., 2012. Gmes sentinel-1 mission. Remote Sens. Environ. 120, 9–24.
van de Leemput, I.A., Dakos, V., Scheffer, M., van Nes, E.H., 2018. Slow recovery from local disturbances as an indicator for loss of ecosystem resilience. Ecosystems 21, 141–152.
Verbesselt, J., Hyndman, R., Zeileis, A., Culvenor, D., 2010. Phenological change detection while accounting for abrupt and gradual trends in satellite image time series. Remote Sens. Environ. 114, 2970–2980.
Verbesselt, J., Umlauf, N., Hirota, M., Holmgren, M., Van Nes, E.H., Herold, M., Zeileis, A., Scheffer, M., 2016. Remotely sensed resilience of tropical forests, nature. Climate Change 6, 1028–1031.
Viana-Soto, A., Aguado, I., Salas, J., Garc'ıa, M., 2020. Identifying post-fire recovery trajectories and driving factors using landsat time series in fire-prone mediterranean pine forests. Remote Sens. 12, 1499.
Vreugdenhil, M., Wagner, W., Bauer-Marschallinger, B., Pfeil, I., Teubner, I., Rudiger, C., Strauss, P., 2018. Sensitivity of sentinel-1 backscatter to vegetation dynamics: an austrian case study. Remote Sens. 10, 1396.
White, J.C., Wulder, M.A., Hermosilla, T., Coops, N.C., Hobart, G.W., 2017. A nationwide annual characterization of 25 years of forest disturbance and recovery for Canada using landsat time series. Remote Sens. Environ. 194, 303–321.
White, J.C., Saarinen, N., Kankare, V., Wulder, M.A., Hermosilla, T., Coops, N.C., Pickell, P.D., Holopainen, M., Hyyppa, J., Vastaranta, M., 2018. Confirmation of post-harvest spectral recovery from landsat time series using measures of forest cover and height derived from airborne laser scanning data. Remote Sens. Environ. 216, 262–275.
White, J.C., Saarinen, N., Wulder, M.A., Kankare, V., Hermosilla, T., Coops, N.C., Holopainen, M., Hyyppa, J., Vastaranta, M., 2019. Assessing spectral measures of post-harvest forest recovery with field plot data. Int. J. Appl. Earth Obs. Geoinf. 80, 102–114.
Wulder, M.A., Masek, J.G., Cohen, W.B., Loveland, T.R., Woodcock, C.E., 2012. Opening the archive: how free data has enabled the science and monitoring promise of landsat. Remote Sens. Environ. 122, 2–10.
Wuyts, B., Champneys, A.R., House, J.I., 2017. Amazonian forest-savanna bistability and human impact. Nat. Commun. 8, 15519.
Zeileis, A., Shah, A., Patnaik, I., 2010. Testing, monitoring, and dating structural changes in ex-change rate regimes. Comp. Stat. Data Anal. 54, 1696–1706.